INTERNATIONAL JOURNAL FOR NUMERICAL METHODS IN FLUIDS
Int. J. Numer. Meth. Fluids 2010; **62**:1155–1168
Published online 23 April 2009 in Wiley InterScience (www.interscience.wiley.com). DOI: 10.1002/fld.2063

Effects of surface waves on hydrodynamic pressures on rigid dams with arbitrary upstream face

Javier Avilés[1,*,†] and Martha Suárez[2]

[1]*Instituto Mexicano de Tecnología del Agua, Jiutepec, Morelos 62550, México*
[2]*Instituto de Ingeniería, UNAM, Apdo. 70-472, Coyoacán 04510, México*

SUMMARY

The effects of surface gravity waves on earthquake-induced hydrodynamic pressures on rigid dams with nonvertical upstream face are examined, taking the compressibility and viscosity of water into account. A simple closed-form solution is obtained by using the Trefftz numerical method. The boundary under study is reduced to the upstream face only and the degrees of freedom of the problem are restricted to the number of trial functions used for analysis. For harmonic base excitation, a number of numerical examples for various geometries of the upstream face are presented. The hydrodynamic pressure distribution, the resultant lateral force and its effective height of application are evaluated. The results are strongly influenced by the upstream shape and, in a lesser degree, by the consideration of surface waves. Copyright © 2009 John Wiley & Sons, Ltd.

Received 20 August 2008; Revised 11 March 2009; Accepted 17 March 2009

KEY WORDS: harmonic base excitation; hydrodynamic pressure; nonvertical upstream face; rigid dam; Trefftz method; surface gravity waves

INTRODUCTION

After the pioneering work of Westergaard [1], the hydrodynamic pressures acting on rigid dams during earthquakes have been extensively studied. Several contributions presented in the literature have addressed diverse aspects of the problem using different methods of solution. For instance, Chopra [2] investigated the effect of water compressibility, Hall and Chopra [3] and Fenves and Chopra [4] examined the influence of the reservoir bottom absorption and Chwang [5] and Avilés and Sánchez-Sesma [6] evaluated the effect of finite reservoir using analytical and numerical methods. By neglecting the compressibility of water, Zangar [7] was the first to study experimentally the influence of the upstream shape, finding that the hydrodynamic pressures are always smaller

*Correspondence to: Javier Avilés, Instituto Mexicano de Tecnología del Agua, Jiutepec, Morelos 62550, México.
†E-mail: javiles@tlaloc.imta.mx

than those for a vertical face. Later, Sharan [8] developed a finite element method and Liu [9] developed an integral equation method to solve problems with complex geometries. A simpler boundary method that makes use of a complete set of Trefftz functions was devised by Avilés and Sánchez-Sesma [10]. With this technique, the degrees of freedom of the problem are restricted to the number of Trefftz functions used in the solution and the boundary under study is reduced to the upstream face only.

The advantages of the Trefftz method for dams with arbitrary upstream face were used by Wu and Yu [11] to study the presence of surface waves in incompressible inviscid fluids. The importance of this effect on the hydrodynamic pressures acting on dams with vertical upstream face was proved by Chwang [12]. The pressures on the dam near the original water surface are influenced to a marked extent by the wave motion at the free surface. The generation of negative pressures implies recurrent separation and subsequent impact between the reservoir and the dam. To represent adequately the effect of surface waves, the compressibility and viscosity of water should be considered. The compressibility introduces internal waves that are amplified at the natural frequencies of the reservoir, while the viscosity tends to attenuate the resonant peaks of the fluid response, as shown by Avilés and Li [13] in the absence of surface waves.

The objective of this paper is to investigate the effect of surface waves on the hydrodynamic pressures exerted on rigid sloping dams by a compressible viscous fluid in an infinitely long reservoir under horizontal ground motion. The solution is obtained by means of a special boundary method that makes use of a complete set of Trefftz functions satisfying all boundary conditions except that at the upstream face. In this way, the pressure distribution is expressed as a linear combination of the natural modes of the reservoir and participation factors. The unknown coefficients of this mode expansion are determined from the continuous treatment of the remaining boundary condition in the least-squares sense. The integration process of the quadratic residual error over the dam–water interface is performed analytically. For several sloping dams subjected to harmonic base excitation, numerical results for the pressure distribution on the dam face, the resultant thrust and the overturning moment are presented, the interpretation of which shows the relative importance of surface and internal waves.

FORMULATION OF PROBLEM

Assuming that the harmonic movement of water is small and irrotational, the flow field in a two-dimensional reservoir can be expressed by a velocity potential function Φ satisfying the reduced wave equation [14]

$$\frac{\partial^2\Phi}{\partial x^2}+\frac{\partial^2\Phi}{\partial y^2}+k^2\Phi=0 \tag{1}$$

such that

$$\dot{u}=-\frac{\partial\Phi}{\partial x},\quad \dot{v}=-\frac{\partial\Phi}{\partial y},\quad p=\rho\frac{\partial\Phi}{\partial t} \tag{2}$$

where $\dot{u}$ and $\dot{v}$ are the particle velocities in the x- and y-directions, respectively, p is the hydrodynamic pressure in the liquid and $k=\omega/C$ is the wavelength parameter of the internal waves, in which ω is the angular frequency of excitation and $C=\sqrt{\lambda/\rho}$ is the velocity of compression waves

DOI: 10.1002/fld

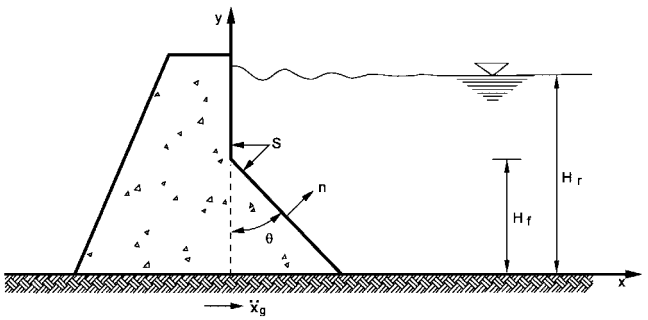

Figure 1. Rigid sloping dam subject to horizontal ground motion.

in water, with λ being Lamé's modulus and ρ the mass density. In what follows, the time-harmonic factor $e^{i\omega t}$ contained in all fields is omitted for brevity.

For an infinitely long dam–reservoir system subjected to the horizontal ground motion x_g, as shown in Figure 1, the boundary conditions to be satisfied are as follows:

(1) At the free surface, Poisson's boundary condition for gravity waves is

$$\left(\frac{\partial^2\Phi}{\partial t^2}+g\frac{\partial\Phi}{\partial y}\right)\Bigg|_{y=H_r}=0 \tag{3}$$

(2) For a reservoir with rigid bottom, the vertical particle velocity is

$$\frac{\partial\Phi}{\partial y}\Bigg|_{y=0}=0 \tag{4}$$

(3) The radiation condition at infinity for the pressure waves is

$$\lim_{x\to\infty}\Phi=0 \tag{5}$$

(4) For a rigid dam with nonvertical upstream face, the normal particle velocity is

$$\frac{\mathrm{d}\Phi}{\mathrm{d}n}\Bigg|_{S}=-\dot{x}_s \tag{6}$$

where g is the acceleration of gravity, H_r is the reservoir height, n is the outward normal direction to the upstream face, S is the dam–water interface and $\dot{x}_s=\dot{x}_g$ if $y\geqslant H_f$ or $\dot{x}_s=\dot{x}_g\cos\theta$ if $y\leqslant H_f$, with H_f being the height of the inclined upstream face and θ the inclination angle with respect to the vertical.

The Voigt model is applied to describe the viscoelastic fluid response. In this way, the internal damping is introduced through replacing the real Lamé's modulus λ by the complex counterpart

$$\lambda^*=\lambda(1+i\eta 2\zeta) \tag{7}$$

where ζ is the viscous damping ratio and $\eta=\omega H_r/C$ is the dimensionless frequency. This equivalent representation of the water viscosity is only a simplification of the real situations, but it does provide a simple and efficient way to simulate the energy loss due to internal dissipation [13].

DOI: 10.1002/fld

SOLUTION BY TREFFTZ METHOD

By introducing a complete set of Trefftz functions, $T_j(x, y)$, which fulfill the governing equation of motion and all boundary conditions except that at the upstream face, the general solution of Equation (1) can be expanded as

$$\Phi = \dot{x}_g \sum_{j=1}^{\infty} \phi_j T_j(x, y) \tag{8}$$

where ϕ_j are unknown complex coefficients to be determined from the remaining boundary condition at the upstream face. The substitution of Equation (8) into Equation (6) results in

$$\left(\sum_{j=1}^{\infty} \phi_j \frac{\mathrm{d}T_j}{\mathrm{d}n} + \frac{\dot{x}_s}{\dot{x}_g} \right) \Bigg|_S = 0 \tag{9}$$

As this equation cannot be solved exactly, the solution will be found in the least-squares sense. Thus, the quadratic residual error in Equation (9) integrated along the dam–water interface is given by

$$E = \int_S \left| \sum_{j=1}^{\infty} \phi_j \frac{\mathrm{d}T_j}{\mathrm{d}n} + \frac{\dot{x}_s}{\dot{x}_g} \right|^2 \mathrm{d}s \tag{10}$$

Notice that the error function is defined as the square of the absolute value of the residual error, since it is a complex-valued function when the compressibility and viscosity of water are considered. The necessary conditions to minimize the error function are

$$\frac{\partial E}{\partial \phi_i^*} = 0, \quad i = 1, 2, \ldots, \infty \tag{11}$$

where the asterisk denotes complex conjugate. Applying Equation (11) over Equation (10), the following Hermitian system of algebraic equations is obtained:

$$\sum_{j=1}^{\infty} \phi_j \int_S \frac{\mathrm{d}T_i^*}{\mathrm{d}n} \frac{\mathrm{d}T_j}{\mathrm{d}n} \mathrm{d}s = -\int_S \frac{\dot{x}_s}{\dot{x}_g} \frac{\mathrm{d}T_i^*}{\mathrm{d}n} \mathrm{d}s, \quad i = 1, 2, \ldots, \infty \tag{12}$$

which in matrix form becomes

$$[F_{ij}]\{\phi_j\} = \{G_i\}, \quad i, j = 1, 2, \ldots, \infty \tag{13}$$

in which:

$$F_{ij} = \int_S \frac{\mathrm{d}T_i^*}{\mathrm{d}n} \frac{\mathrm{d}T_j}{\mathrm{d}n} \mathrm{d}s \tag{14}$$

$$G_i = -\int_S \frac{\dot{x}_s}{\dot{x}_g} \frac{\mathrm{d}T_i^*}{\mathrm{d}n} \mathrm{d}s \tag{15}$$

These equations can be integrated out analytically, resulting in closed-form expressions for the matrix coefficients F_{ij} and G_i. Since Equation (13) includes infinite equations, it cannot be solved exactly. The solution is obtained by truncating the system of equations at a given value $i, j = 1, 2, \ldots, N$.

The task now is to derive the Trefftz functions that fulfill both the equation of motion as well as the boundary conditions at the free surface, reservoir bottom and infinity. By using the method of

DOI: 10.1002/fld

separation of variables, the natural modes of water propagating horizontally can be expressed as

$$T_j(x, y) = \mathrm{e}^{-\mu_j x} \cos \lambda_j y \tag{16}$$

in which

$$\mu_j = \sqrt{\lambda_j^2 - k^2} \tag{17}$$

where μ_j and λ_j are horizontal and vertical propagation constants, respectively. For a dissipative fluid, μ_j is a complex-valued quantity in general. The square root sign in this expression refers to that for which the real part of μ_j is positive, representing an evanescent mode that satisfies the radiation condition at infinity. For a nondissipative fluid and values of $k > \lambda_j$, i.e. for exciting frequencies greater than the natural frequency of the mode being considered, the value of μ_j is imaginary indicating the absence of radiation damping in this range.

From the form of Equation (16), the boundary condition at the reservoir bottom is automatically fulfilled. When the boundary condition at the free surface is satisfied, the following dispersion relation is found:

$$\lambda_j H_r \tan \lambda_j H_r = -\sigma \tag{18}$$

where $\sigma = \omega^2 H_r / g$ is the surface-wave parameter. For a given value of σ, the roots of Equation (18) can be obtained from an iterative process, starting with an initial guess for $\lambda_j H_r$ and stopping when the difference between two successive iterations is less than a specified tolerance. If $\sigma = 0$, Equation (18) reduces to $\sin \lambda_j H_r = 0$, whose roots are $\lambda_j H_r = j\pi$; whereas if $\sigma = \infty$, Equation (18) reduces to $\cos \lambda_j H_r = 0$, whose roots are $\lambda_j H_r = (2j-1)\pi/2$. For $\sigma < 1$ and $\sigma > 10$, these solutions can be used as a initial values of iteration, respectively, when applying the well-known Newton–Raphson method for root finding. Otherwise, the trial roots may be approximated as

$$\lambda_j H_r \approx \frac{4j-1}{2} \frac{\pi}{2} \tag{19}$$

corresponding to an intermediate value between the lower and upper bounds that bracket the true roots.

Using the Trefftz functions given by Equation (16), the integration of Equations (14) and (15) resulted in the following expressions after extensive mathematical manipulations:

$$G_i = \frac{\mu_i^*}{\lambda_i} [\sin \lambda_i H_r - \sin \lambda_i H_f] + \frac{\sec \theta}{\lambda_i^2 + \mu_i^{*2} \tan^2 \theta} \times [\mu_i^* \lambda_i \sec^2 \theta \sin \lambda_i H_f + (\lambda_i^2 - \mu_i^{*2}) \tan \theta \, (\mathrm{e}^{-\mu_i^* H_f \tan \theta} - \cos \lambda_i H_f)] \tag{20}$$

$$F_{ij} = \frac{\sec \theta}{2 L_{ij}^+ L_{ij}^-} (A_{ij} + B_{ij} + C_{ij} + D_{ij}) + E_{ij} \tag{21}$$

in which

$$A_{ij} = \mu_i^* \mu_j [M_{ij}^- L_{ij}^+ + M_{ij}^+ L_{ij}^- - \mu'_{ij} K_{ij} (L_{ij}^+ + L_{ij}^-)] \tag{22}$$

$$B_{ij} = \lambda_i \lambda_j \tan^2 \theta [M_{ij}^- L_{ij}^+ - M_{ij}^+ L_{ij}^- - \mu'_{ij} K_{ij} (L_{ij}^+ - L_{ij}^-)] \tag{23}$$

DOI: 10.1002/fld

$$C_{ij}=\mu_i^*\lambda_j\tan\theta[N_{ij}^+L_{ij}^--N_{ij}^-L_{ij}^++K_{ij}(\lambda_{ij}^+L_{ij}^--\lambda_{ij}^-L_{ij}^+)] \tag{24}$$

$$D_{ij}=\lambda_i\mu_j\tan\theta[N_{ij}^+L_{ij}^-+N_{ij}^-L_{ij}^++K_{ij}(\lambda_{ij}^+L_{ij}^-+\lambda_{ij}^-L_{ij}^+)] \tag{25}$$

$$E_{ij}=\frac{\mu_i^*\mu_j}{2}\left[\delta_{ij}\left(H_r-H_f+\frac{\sin\lambda_{ij}^+H_r-\sin\lambda_{ij}^+H_f}{\lambda_{ij}^+}\right)\right.$$
$$\left.+(1-\delta_{ij})\left(\frac{\sin\lambda_{ij}^+H_r-\sin\lambda_{ij}^+H_f}{\lambda_{ij}^+}+\frac{\sin\lambda_{ij}^-H_r-\sin\lambda_{ij}^-H_f}{\lambda_{ij}^-}\right)\right] \tag{26}$$

where δ_{ij} is the Kronecker delta ($=1$ if $i=j$, $=0$ if $i\neq j$). The rest of the terms appearing in Equations (22)–(26) are equal to:

$$K_{ij}=\exp(-\mu_{ij}'H_f) \tag{27}$$

$$L_{ij}^{\pm}=\mu_{ij}'^2+\lambda_{ij}^{\pm 2} \tag{28}$$

$$M_{ij}^{\pm}=\mu_{ij}'\cos\lambda_{ij}^{\pm}H_f+\lambda_{ij}^{\pm}\sin\lambda_{ij}^{\pm}H_f \tag{29}$$

$$N_{ij}^{\pm}=\mu_{ij}'\sin\lambda_{ij}^{\pm}H_f-\lambda_{ij}^{\pm}\cos\lambda_{ij}^{\pm}H_f \tag{30}$$

$$\mu_{ij}'=(\mu_i^*+\mu_j)\tan\theta \tag{31}$$

$$\lambda_{ij}^{\pm}=\lambda_i\pm\lambda_j \tag{32}$$

We see that, based on the Trefftz formulation, the analysis leads to a closed-form solution for dams with a combination of vertical and sloping faces, since in this case the curvilinear integrals in Equations (14) and (15) are solved analytically. For arbitrary geometries; however, these integrals should be performed numerically.

RESULTS AND INTERPRETATIONS

The results presented herein are for the pressure distribution on the dam face, the resultant thrust and the overturning moment due to harmonic base excitation. It is apparent from Equations (2), (8) and (16) that the dam pressure at any arbitrary elevation is given by

$$p_s=\rho\ddot{x}_g\sum_{j=1}^{N}\phi_j e^{-\mu_j x}\cos\lambda_j y,\quad \begin{array}{ll} x=(H_f-y)\tan\theta & \text{if } y\leqslant H_f \\ x=0 & \text{if } y\geqslant H_f\end{array} \tag{33}$$

From this, it is a simple matter to calculate the shear force and bending moment exerted on the dam by integration. In particular, the base shear per unit of dam length is given by

$$q_s=\int_o^{H_f}p([H_f-y]\tan\theta,y)\,dy+\int_{H_f}^{H_r}p(0,y)\,dy \tag{34a}$$

DOI: 10.1002/fld

$$q_s = \rho \ddot{x}_g \sum_{j=1}^{N} \phi_j \left[\frac{\sin \lambda_j H_r - \sin \lambda_j H_f}{\lambda_j} + \frac{1}{\lambda_j^2 + \mu_j^2 \tan^2 \theta} \times \left(\mu_j \tan\theta \cos \lambda_j H_f + \lambda_j \sin \lambda_j H_f - \frac{\mu_j \tan\theta}{e^{\mu_j H_f \tan\theta}} \right) \right] \tag{34b}$$

and the corresponding base moment is given by

$$m_s = \int_o^{H_f} p([H_f - y]\tan\theta, y) y \, dy + \int_{H_f}^{H_r} p(0, y) y \, dy \tag{35a}$$

$$m_s = \rho \ddot{x}_g \sum_{j=1}^{N} \phi_j \left[\frac{\cos \lambda_j H_r - \cos \lambda_j H_f}{\lambda_j^2} + \frac{H_r \sin \lambda_j H_r - H_f \sin \lambda_j H_f}{\lambda_j} + \frac{(\lambda_j^2 - \mu_j^2 \tan^2\theta)(\cos \lambda_j H_f - e^{-\mu_j H_f \tan\theta}) - 2\mu_j \lambda_j \tan\theta \sin \lambda_j H_f}{(\lambda_j^2 + \mu_j^2 \tan^2\theta)^2} + \frac{\mu_j H_f \tan\theta \cos \lambda_j H_f + \lambda_j H_f \sin \lambda_j H_f}{\lambda_j^2 + \mu_j^2 \tan^2\theta} \right] \tag{35b}$$

Let $C_{pi} = \mathrm{Re}(p_s)/\rho \ddot{x}_g H_r$ and $C_{po} = \mathrm{Im}(p_s)/\rho \ddot{x}_g H_r$ the in-phase and out-of-phase components of the total pressure coefficient $C_p = \sqrt{C_{pi}^2 + C_{po}^2}$. The variation of these coefficients is plotted against

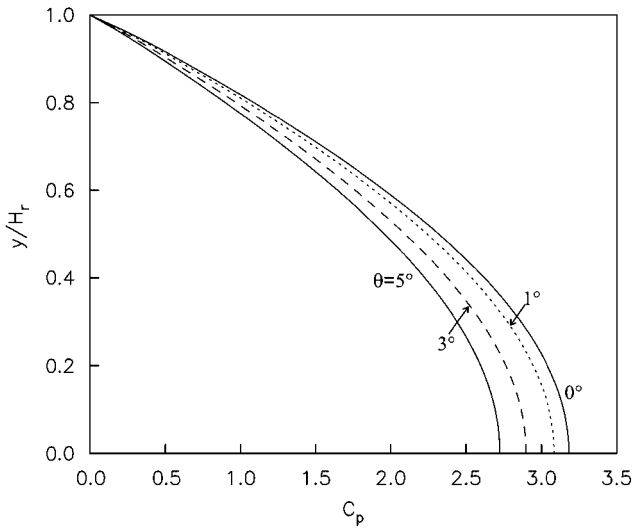

Figure 2. Convergence of the present solution toward the exact one [2] for vertical upstream face, when decreasing the value of θ while H_f/H_r is fixed at 1; results are for $\zeta = 2\%$ and $\omega/\omega_1 = 1$.

DOI: 10.1002/fld

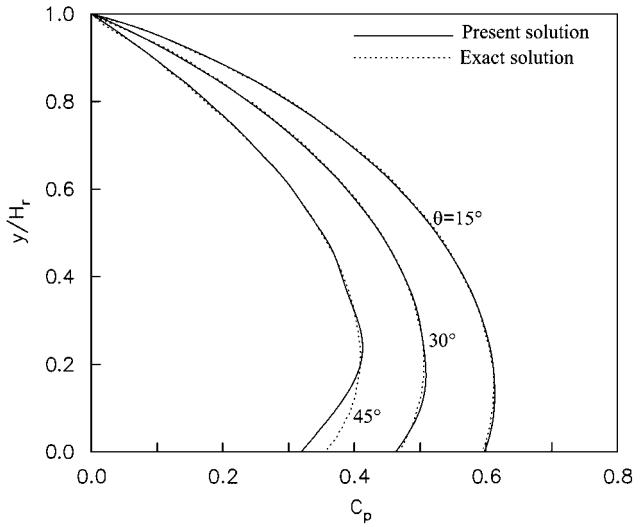

Figure 3. Comparison of the present solution with the exact one [15] for $H_f/H_r=1$ and different values of θ; results are for $\zeta=0$ and $\omega/\omega_1=0$ in the absence of surface waves.

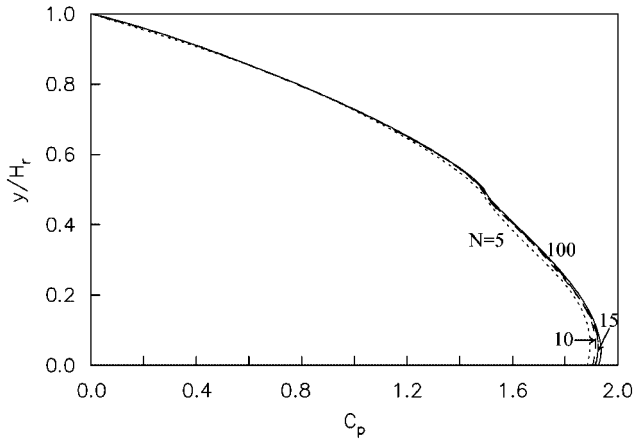

Figure 4. Convergence of the numerical solution with increasing the number of terms N for a sloping dam with $H_f/H_r=0.5$ and $\theta=30°$; results are for $\zeta=2\%$ and $\omega/\omega_1=1$.

the dimensionless distance y/H_r from the base, whereas the magnitude of the force and moment coefficients $C_q=|q_s|/\rho\ddot{x}_g H_r^2$ and $C_m=|m_s|/\rho\ddot{x}_g H_r^3$ is plotted against the frequency ratio ω/ω_1, with $\omega_1=\pi C/2H_r$ being the fundamental natural frequency of the reservoir.

When $\theta=0$ or $H_f=0$, Equation (13) is reduced to a diagonal system of equations, the solution of which leads to the following expression for the hydrodynamic pressure:

$$p(x,y,\omega)=\frac{2\rho\ddot{x}_g}{H_r}\sum_{j=1}^{N}\frac{(-1)^{j-1}}{\mu_j\lambda_j}\mathrm{e}^{-\mu_j x}\cos\lambda_j y \tag{36}$$

DOI: 10.1002/fld

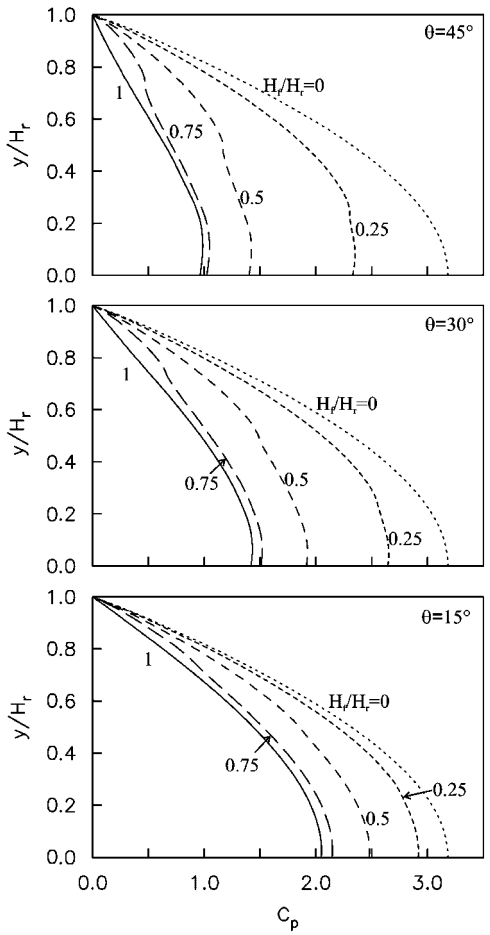

Figure 5. Variation of the total pressure coefficient with depth for different values of the sloping angle θ and the height ratio H_f/H_r; results are for $\zeta=2\%$ and $\omega/\omega_1=1$.

which has the same form as that derived by Chopra [2] for vertical upstream face. To the authors' knowledge, this is the only published exact solution to the problem of compressible fluid. The numerical verification of the proposed method is shown in Figure 2 for $H_f=H_r$ and descending values of θ, starting with 5° and ending with 1°. These results tend uniformly to the exact solution for the limiting case of $\theta=0$. When considering incompressible fluid, we have that $k=\omega/C=0$ and hence $\mu_j=\lambda_j$ according to Equation (17). The results obtained under this assumption for $H_f=H_r$ and $\theta=15, 30$ and 45° are compared in Figure 3 with the exact results obtained by Chwang [15]. The agreement between the results is very good, except close to the bottom for high-sloping angles.

In order to prove the convergence of solution, a sloping dam with $H_f/H_r=0.5$ and $\theta=30°$ was analyzed using $N=5, 10, 15$ and 100 terms of the series expansion. The results of Figure 4 demonstrate a rapid convergence to a unique solution only with a few number of terms. For

DOI: 10.1002/fld

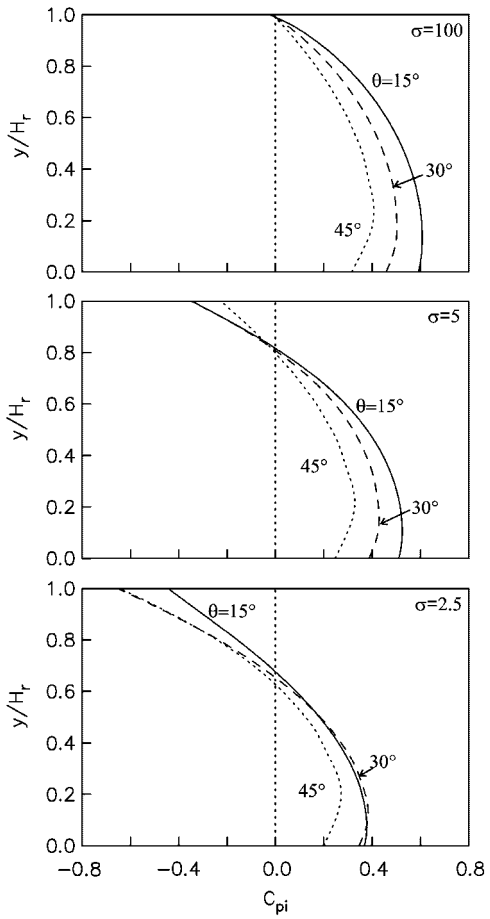

Figure 6. Variation of the in-phase pressure coefficient with depth for different values of the surface-wave parameter σ and the sloping angle θ; results are for $\zeta=2\%$ and $H_f/H_r=1$.

good accuracy of calculations, it is thus sufficient to limit the number of terms to $N=15$ for any geometry of the dam face.

The influence of the upstream shape on the pressure distribution is observed in Figure 5 for dams with different combinations of vertical and sloping faces. The coefficient C_p was calculated for the combinations of $\theta=15, 30$ and 45° with $H_f/H_r=0, 0.25, 0.5, 0.75$ and 1. It can be seen that the largest and smallest values of pressure are generated for the cases of vertical ($H_f/H_r=0$) and fully inclined ($H_f/H_r=1$) face, respectively. The hydrodynamic pressure for any partially inclined face is bounded by these two solutions.

Two sloping dams were analyzed to show the effect of surface waves on the pressure distribution. The first has a fully inclined face with $\theta=15, 30$ and 45° and the second is partially inclined with $H_f/H_r=0.5$ and the same sloping angles. For the values of σ used in the calculations, it is found that $C_{pi}\neq 0$ and $C_{po}=0$. This happens when $\omega<\omega_1$ according to Equation (17). It is shown in Figures 6 and 7 that the dam pressure at the water surface is no longer zero for $\sigma=2.5$ and 5.

DOI: 10.1002/fld

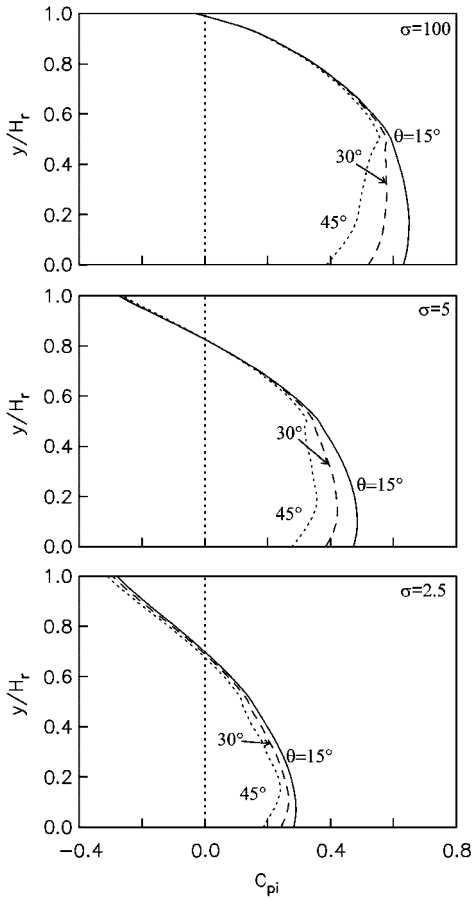

Figure 7. Variation of the in-phase pressure coefficient with depth for different values of the surface-wave parameter σ and the sloping angle θ; results are for $\zeta = 2\%$ and $H_f/H_r = 0.5$.

For $\sigma = 100$, however, surface waves prove to be irrelevant. The generation of negative pressures at the top is accompanied by the reduction in positive pressures at the base, with the former effect being more critical for the fully inclined face and the latter for the partially inclined face. Both actions are in phase with the dam motion.

For the same cases, the coefficients C_q and C_m were calculated in the frequency range between 0 and 4 times ω_1. Figures 8 and 9 show that the shapes of these coefficients are very similar, but with considerable changes in their magnitudes. As seen before, the effect of surface waves is important for frequencies that are much smaller than the first critical frequency. Conversely, the major effect of internal waves due to the compressibility of water occurs precisely at this resonance frequency. It should be noted that the resultant thrust around $\omega/\omega_1 = 1$ reduces with increasing the value of θ, specially for the fully inclined face, which is the most favorable geometry.

The effective height $\tilde{h} = C_m/C_q$ is the elevation of the point of action of the resultant thrust normalized with respect to the reservoir height. The resulting curves for this parameter are plotted

DOI: 10.1002/fld

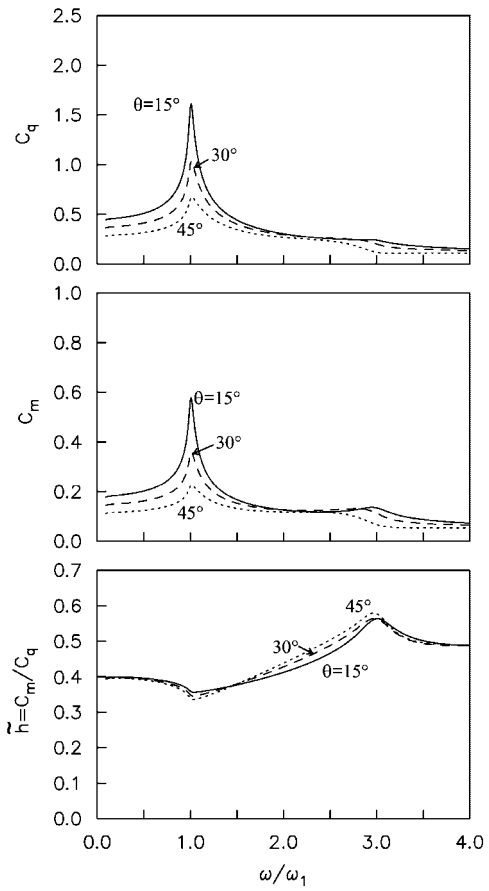

Figure 8. Variation of the force and moment coefficients with frequency, as well as of the effective height, for different values of the sloping angle θ; results are for ζ=1% and H_f/H_r=1.

in Figures 8 and 9 as well. The effective height for the hydrodynamic thrust should be compared with the value of $\frac{1}{3}$ for the hydrostatic thrust. The base-moment amplitude may conveniently be expressed as the product of the base-shear amplitude and the effective height. The dynamic values of $\tilde{h}$ show a small deamplification at $\omega/\omega_1 = 1$ and a great amplification at $\omega/\omega_1 = 3$, corresponding to the second critical frequency.

CONCLUSIONS

A closed-form solution for hydrodynamic pressures on rigid sloping dams under the presence of surface waves in compressible fluid has been presented. The main advantage of this solution is that the computational effort is independent of the extent of the reservoir. A special boundary method

DOI: 10.1002/fld

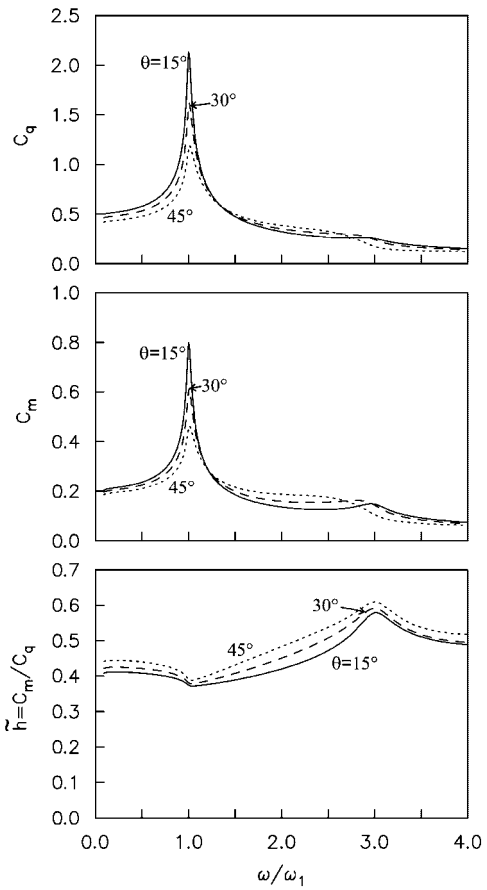

Figure 9. Variation of the force and moment coefficients with frequency, as well as of the effective height, for different values of the sloping angle θ; results are for $\zeta = 1\%$ and $H_f/H_r = 0.5$.

was applied, which makes use of a complete set of Trefftz functions that satisfy all boundary conditions except that at the upstream face.

For harmonic base excitation, it was found that the water pressure on dams with partially inclined face is bounded by the solutions for the limiting cases of vertical and fully inclined face. As a consequence of the surface waves, negative pressures arise at the dam's top accompanied by the reduction of pressure at the base, with the former effect being more critical for the fully inclined face and the latter for the partially inclined face.

The effects of surface and internal waves are significant at different frequency ranges. While the former is observed at frequencies that are much smaller than the first critical frequency, the latter appears at this resonance frequency. The effect of surface waves was found to be small when compared with that of internal waves. The resultant of the hydrodynamic pressures around the first critical frequency was shown to be reduced with an increase in the sloping angle of the dam face. The point of action for the hydrodynamic force lies at an elevation that varies between 0.35 and 0.6 of the reservoir height, compared with the value of $\frac{1}{3}$ for the hydrostatic force.

DOI: 10.1002/fld

In its present form, the proposed method is very efficient and simple for dams with a combination of vertical and sloping faces. Nevertheless, the method may also be suitable for arbitrary geometries. In this case, the integration equations for the boundary conditions should be carried out numerically.

REFERENCES

1. Westergaard HM. Water pressures on dams during earthquakes. *Transactions of the ASCE* 1933; **98**:418–472.
2. Chopra AK. Hydrodynamic pressures on dams during earthquakes. *Journal of the Engineering Mechanics Division* (ASCE) 1967; **93**:205–223.
3. Hall JF, Chopra AK. Two dimensional dynamic analysis of concrete gravity and embankment dams including hydrodynamic effects. *Earthquake Engineering and Structural Dynamics* 1982; **10**:305–332.
4. Fenves G, Chopra AK. Effects of reservoir bottom absorption on earthquake response of concrete gravity dams. *Earthquake Engineering and Structural Dynamics* 1983; **11**:809–829.
5. Chwang AT. Hydrodynamic pressure on an accelerating dam and criteria for cavitation. *Journal of Engineering Mathematics* 1979; **13**:143–152.
6. Avilés J, Sánchez-Sesma FJ. Water pressures on rigid gravity dams with finite reservoir during earthquakes. *Earthquake Engineering and Structural Dynamics* 1989; **18**:527–537.
7. Zangar CN. Hydrodynamic pressures on dams due to horizontal earthquakes. *Proceedings of the Society on Experimental Stress Analysis* 1953; **10**:93–102.
8. Sharan SK. Finite element analysis of unbounded and incompressible fluid domains. *International Journal for Numerical Methods in Engineering* 1985; **21**:1659–1669.
9. Liu PLF. Hydrodynamic pressures on rigid dams during earthquakes. *Journal of Fluid Mechanics* 1986; **165**: 131–145.
10. Avilés J, Sánchez-Sesma FJ. Hydrodynamic pressures on dams with nonvertical upstream face. *Journal of Engineering Mechanics* (ASCE) 1986; **112**:1054–1061.
11. Wu YC, Yu DJ. Trefftz method for hydrodynamic pressure on rigid dams with non-vertical upstream face. *International Journal for Numerical Methods in Fluids* 1989; **9**:1–7.
12. Chwang AT. Effect of stratification on hydrodynamic pressures on dams. *Journal of Engineering Mathematics* 1981; **15**:49–63.
13. Avilés J, Li X. Analytical–numerical solution for hydrodynamic pressures on dams with sloping face considering compressibility and viscosity of water. *Computers and Structures* 1998; **66**:481–488.
14. Newmark NM, Rosenblueth E. *Fundamentals of Earthquake Engineering*. Prentice-Hall: New Jersey, 1971.
15. Chwang AT. Hydrodynamic pressures on sloping dams during earthquakes. Part 2. Exact theory. *Journal of Fluids Mechanics* 1978; **87**:343–348.

DOI: 10.1002/fld